Fabrication of Micro Lens Array by Excimer Laser Micromachining

Syed Nadeem Akhtar, Shashank Sharma and J. Ramkumar

Abstract Micro Lens arrays are widely used in optical devices such as photo-sensors, digital projectors, photovoltaic cells, 3D imaging etc. These have traditionally been fabricated by photolithography, moulding and embossing, reactive ion etching and electroforming. These processes are wet processes and require expensive setup and running cost. A novel method is presented in this work that allows fabrication of micro lens array using excimer laser micromachining. The fabrication has been done using mask projection with work piece scanning. A KrF excimer laser has been used to micro machine lenses on a poly (methyl methacrylate) substrate. The surface profile of the lens array is measured and then related to the laser-material coupling and the energy of the laser pulses. Using this method, it is possible to fabricate micro lenses down to a diameter of 5 μm over a considerably large area.

Keywords Excimer laser · Lens array · Ablation rate · Micromachining

1 Introduction

Researchers had begun to investigate the mechanism of laser ablation in the early 1960s with tools like high speed photography and atomic force microscopy. Ready (1965), for example had put in efforts to study, both experimentally and analytically, the laser ablation using classical heat transfer and thermodynamic principles. The observations started out with basic measurements of depth of ablation and understanding its correspondence with analytically calculated data. Since then, the study of laser ablation mechanisms, for various materials, has progressed to the extent that advanced techniques like time-resolved spectroscopy and molecular dynamics simulations are able to observe and predict the escape velocity of ablated

S.N. Akhtar (✉) · S. Sharma · J. Ramkumar
Department of Mechanical Engineering, Indian Institute of Technology Kanpur, Kanpur 208016, India
e-mail: snadeem@iitk.ac.in

© Springer India 2015

S.N. Joshi and U.S. Dixit (eds.), *Lasers Based Manufacturing*,
Topics in Mining, Metallurgy and Materials Engineering,
DOI 10.1007/978-81-322-2352-8_12

fragments, their composition and time duration of ablation (Dijkkamp et al. 1987; Srinivasan et al. 1986, 1995).

This paper reviews the observations and findings relating to the mechanism of ablation of polymers when irradiated by nanosecond UV lasers. Excimer lasers are a part of this category and have been considered for this review. The paper first introduces the basic parameters of lasers that play a significant role in the ablation process. Definition of key terminologies related to the process and properties of materials are then discussed. This is followed by a discussion on mechanisms active during the excimer laser ablation of polymers and the various pathways and products as a result of this ablation.

2 Parameters of Laser Radiation

A laser radiation is characterized by certain key parameters. Concerning lasers used in machining of materials, these parameters are the wavelength of radiation, the nature of radiation (continuous or pulsed), the duration of the pulse and the quality of the beam. Wavelength (λ) determines the energy carried by individual photons in the laser beam and hence the kind of interaction these photons will have with the material. Large wavelength lasers, like CO_2 lasers (λ = 10.6 μm), mainly cause ablation by a thermal process because the photons do not carry enough energy to cause any other effect. Short wavelength lasers, like F_2 lasers (λ = 157 nm), mainly cause ablation by a photolytic process wherein the photons are directly involved in breaking of bonds within the material. A description of the various types of excimer lasers, their wavelengths and photon energies is given in Table 1. Since we are concerned with UV lasers (λ < 400 nm), photolytic ablation process will dominate the discussion.

3 Key Terminologies in Laser Material Interactions

When a laser radiation is incident on a material most of the photons get absorbed by the electrons present in the outermost shell of atoms in the top skin layer. The thickness of the skin layer, also called the optical penetration depth (δ), is $2/\alpha$ where

Table 1 Excimer lasers and the associated wavelengths and photon energies

Laser	Wavelength (nm)	Photon energy (eV)
XeF	351	3.53
XeCl	308	4.03
KrF	248	5.00
KrCl	222	5.50
ArF	193	6.42
F_2	157	7.43

From Meijer (2004), reprinted with permission

'α' is the absorption coefficient of the material for the particular wavelength. The optical penetration depth for polymers is about 200 nm. The time it takes for the photons to get absorbed is called the photon absorption time (t_a) and is of the order of 1 fs. These photons cause the electrons to get excited. The time it takes for the excited electrons to relax to their previous state is called the electron relaxation time (or electron cooling time, t_e) and is of the order of 1 ps. After 1 ps of irradiation, the electrons relax and pass on the energy to the lattice in the form of heat. This heat diffuses into the material at the rate determined by the thermal diffusivity (κ) and thermal conductivity (k) of the material (Meijer 2004; Choudhary 2012; Meijer et al. 2002). The depth through which the heat diffuses into the material in a certain time 't' is called the thermal diffusion depth (d) and is given by $d = \sqrt{(4\kappa t)}$.

The pulse duration is a property of the laser radiation. However, the pulses are classified as short or ultra short based on whether the optical penetration depth is more or less than the thermal diffusion depth (in time 't_e'), respectively. Generally speaking, pulses with duration less than 1 ps are called ultra short pulses. An often used term in laser machining is 'fluence'. Fluence is defined as the irradiated energy per pulse per unit area of the material and its units are J/cm^2. Ablation is noticeable only above a certain value of fluence (depending on the material) and this value is called the threshold fluence (F_{th}). Researchers have over time realized that instead of fluence (that makes no reference to the time in which the energy is delivered), intensity better describes the effect of radiation (Srinivasan et al. 1995; Jensen 2004). Intensity, then, is defined as average power per pulse per unit area and its units are W/cm^2. Several parameters affect the mechanism and extent of laser ablation in polymers, and some of those are mentioned in Table 2 for some common polymers.

4 Mechanism of Laser Ablation of Polymers

For ablation of polymers by nanosecond UV laser, the process is a combination of thermal (pyrolytic) and photo (photolytic) ablation. Since the pulse duration here is much larger than that of ultra short pulses, non-linear processes like multi-photon absorption do not occur (Srinivasan et al. 1986). Pyrolytic ablation starts with

Table 2 Some common polymers and their absorption coefficients and thermal diffusivities

Polymer	Absorption coefficient (α, μm^{-1}) at 248 nm	Thermal diffusivity (κ, m^2/s)
Polycarbonate	1	0.144×10^{-6}
Polypropylene	–	0.096×10^{-6}
Polyimide	22	0.122×10^{-6}
PMMA	0.0063	0.115×10^{-6}

From Meijer (2004), Jensen (2004), Tsutsumi and Kiyotsukuri (1988), reprinted with permission

absorption of the incident photons and electronic excitation of the material. It however proceeds via random distribution of this energy amongst the various degrees of freedom of the constituents (molecules) which in turn leads to heating of the material. The heated material ablates via both melt/vaporization and thermal degradation (bond-scission leading to fragmentation) routes. Both these processes happen in the ground state of the constituents (Dyer 2003). This is significantly observed for higher wavelength (low energy photons) and longer pulse lasers ($t_p \geq 1$ μs). The two basic reasons for pyrolytic ablation are that, firstly, the energy from the low energy photons is transferred to the electrons and then to the lattice in the form of heat energy. The photons do not carry enough energy to cause any other effect, e.g. breaking the covalent bonds in the material. Secondly, the duration of irradiation (t_p) is significantly larger than the electron relaxation time (t_e) and the energy from the photons begins to travel into the material during the irradiation, leading to heating of the vicinity of the area being irradiated. Pyrolytic ablation often leads to a heat affected zone (HAZ) around the irradiated area, thermal degradation and evidence of melt flow. These effects, however, are generally not significantly observed in case of ablation of polymers with nanosecond lasers.

Photolytic ablation is a photo-chemical process that involves bond breaking and formation with the aid of incident photons. Polymers are composed of elements (like C, O, H, N, F, Cl etc.) joined together by covalent bonds. The incident photons, if sufficiently energetic, can modify the bond structure within the material leading to bond-scission or cross-linking effects. The intensity of radiation is so high in nanosecond UV lasers that the numbers of bonds that are broken are several orders of magnitude higher than those that are formed. This, however, requires that the incident photons carry sufficient energy to break the covalent bonds. Typical bond energies of some common covalent bonds are given in Table 3 that may be compared to the energy of photons as mentioned in Table 1. Upon comparison it can be inferred that UV lasers ablate majorly through photolytic ablation owing to the high energy of the photons, although this will be further discussed in the following section. The incoming photons break the covalent bonds in the long polymer chains resulting in generation of several smaller chains present within the same volume (Meijer 2004; Jensen 2004). This fragmentation or decomposition of the polymer happens when the reactants are in electronically excited state (Dyer 2003). When the number of chains in a unit volume exceeds a certain value, meaning that when the bond density in that volume decreases below a critical value, the smaller chains explode out in the form of vapor and small particles. This explosion leads to expelling of the material and ablation.

Table 3 Bonds and their bond energies

Bonds	Bond energy (eV)
Si–Si, Cl–Cl	1.8–3.0
C–N, C–C	3.0–3.5
C–O, C–H	4.5–4.9
C=C, C=O	7.0–8.0

From Meijer (2004), reprinted with permission

5 Analysis and Observations

5.1 Nature of Ablation

Pure photolytic ablation, also called cold ablation, is unlikely with nanosecond lasers. Several researchers have observed signatures of both pyrolytic and photolytic ablation in polymers. Dijkkamp et al. (1987) observed through time resolved reflectivity measurements that the ablation of poly-methylmethacrylate (PMMA) and poly (3-butenyltrimethylsilane sulfone) (PBTMSS) was entirely due to pyrolytic ablation with KrF excimer laser. Feng et al. studied the ablation of polypropylene (PP) with KrF excimer laser. They observed that even with fluence near the ablation threshold of the polymer, ablation was observable on the surface. Although the ablation was due to expelling of fragments generated after polymer chain scissions, the scission was caused not directly by the photons but by the heating of the polymer surface by the radiation. A rim of solidified polymer was observed around the ablated crater suggesting that polymer had melted and flown out of the surface and then resolidified around the crater (see Fig. 1). The observation that the rim increased in size with increase in fluence and the number of pulses suggests accumulation of heat with higher fluence and number of pulses. Dyer (2003) observes that polymers that are thermally robust (like polyimide) have been confirmed to ablate by extensive fragmentation, indicating that photolytic ablation resulting in covalent bond scission was the active mechanism.

Relative importances of the two ablation mechanisms have also been studied by researchers. Feng et al. (2000) found that photo ablation dominates at very low or very high fluence. For the fluence range generally used in ablation pyrolytic ablation was found to be dominant. However, since laser ablation employs irradiation with several pulses, a cumulative effect of both processes is always observed. Jensen suggested that the relative dominance can be checked by comparing the values of the optical and the thermal penetration depths of a material for a particular wavelength and pulse duration.

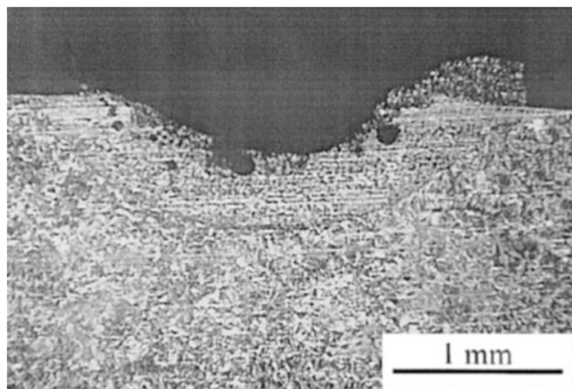

Fig. 1 The cross sectional micrograph of an ablated crater in PP showing the rim formation (from Feng et al. (2000), reprinted with permission)

5.2 Plume Interaction During the Laser Pulse

Pulses of KrF excimer laser, for example, last for about 20 ns. Immediately after a pulse hits the material, a high temperature plasma plume is formed that contains gaseous components, small fragments and radicals. This plume is continuously fed by the fragments being expelled out from the material surface during the pulse. Since the plume is developed almost immediately after the pulse hits the material, a significant portion of the pulse strikes the plume while on its way to the material surface. The plume (i.e. the species present in the plume) are known to significantly absorb the incoming radiation and letting only a small portion of it through. Then the effective absorption coefficient of the polymer is considerably reduced and leads to a lower extent of ablation (etch rate). For a highly absorbing plume, low fluence results in efficient ablation of the polymer surface and vice versa. Using a high fluence, in this case, leads to heating of the plume and hence to undesirable thermal effects (Dyer 2003).

5.3 Ablation Rate and Threshold

Ablation rate is one of the most studied parameters in laser machining of polymers. The ablation rate is also called the etch rate and is defined as the depth (ablated) per pulse of laser. It is measured either in nm or in μm and is an average quantity. It has been always observed that the threshold fluence must be exceeded in order for ablation to set in. This is required across the entire band of wavelengths. For sub-100 ns pulse duration lasers, the fluence threshold is independent of the pulse duration. This, however, is not true for longer duration pulses (Dyer 2003). It is still a matter of investigation and debate as to whether a true ablation threshold exists for a material. The authors of this paper have measured the etch depth and ablation rate of biaxially-oriented polyethylene terephthalate (boPET) when irradiated with KrF excimer laser (Akhtar 2013). The measurements are shown in Fig. 2. The ablation rate was found to increase with fluence and was constant up to a certain number of pulses for the same fluence. Etching of polymers has been observed in the vicinity (lower) of ablation thresholds. In their study of ablation of polyimide using excimer lasers, Kuper et al. (1993) found smooth curves for etch rate versus fluence, suggesting the absence of any kind of ablation threshold. A sharp threshold has, however, been observed with ArF (193 nm) laser while machining polyimide. A clearer description of polymer behaviour at high temperatures or energy densities is difficult at this time due to the absence of experimental data regarding this process. In the domain of photolytic ablation, if a minimum of 'n' bonds per unit volume of the material need to be broken to initiate ablation, the threshold fluence, F_{th}, can be expressed as

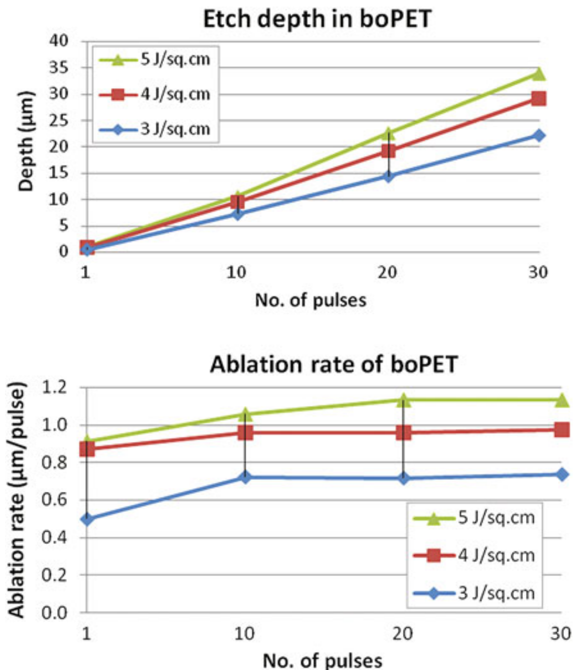

Fig. 2 Ablation depth (*top*) and ablation rate (*bottom*) plotted as a function of the number of pulses for various fluences during machining of boPET by KrF excimer laser [from Akhtar et al. (2013)]

$$F_{th} = \frac{nhv}{\eta\alpha(1 - R)} \tag{1}$$

where η is the quantum efficiency of bond-scission, hv is the photon energy and R is the surface reflectivity. The quantum efficiency of bond scission increases with decrease in wavelength. Hence η for ArF laser is more than that for KrF laser. The η for KrF, however, can be increased by increasing the temperature so that the photochemical processes are accelerated (Srinivasan et al. 1986). In the domain of pyrolytic ablation,

$$F_{th} = \frac{C(T_{th} - T_s)}{\alpha(1 - R)} \tag{2}$$

where 'C' is the volumetric specific heat capacity of the material, T_{th} is the minimum temperature required to be reached to initiate thermal degradation of the material, and T_s is the surface temperature of the material (Dyer 2003). The intensity of radiation at a depth 'y' into the material, $I(y)$, follows the Beer's law of attenuation, $I(y) = I(0)e^{-\alpha y}$, where $I(0)$ is the intensity at the surface. The etch rate (depth per pulse, 'd') shows a logarithmic dependence on the fluence and follows the relation, $d = \alpha^{-1}\ ln(F/F_{th})$, where α is experimentally determined. The etch depth varies linearly with the log of fluence for values of fluence ranging between F_{th} and a certain upper limit. For a constant fluence, the etch depth varies linearly

with the number of pulses. Decrease of etch rate at high fluence is due to secondary absorption of incoming photons by the expelled products (present in the plume) and distribution of the irradiation over the walls of the ablated crater. Also, low energy pulses do not break enough number of C–C bonds and hence lead to small etch depths. Moderate energy pulses are able to break enough number of C–C bonds that leads to efficient ablation and comparatively greater etch depth. High energy pulses break a large number of C–C bonds but over the same polymer mass (albeit into smaller polycarbon fragments that explode out) leading to almost the same etch depth. Hence beyond a particular pulse energy (fluence) the efficiency of photolytic ablation levels off (Dayal et al. 2013).

5.4 Mask Projection Technique

Excimer lasers are widely used with mask projection. The technique involves use of a mask, through which the laser beam passes before hitting the work piece, as shown in Fig. 3. A beam delivery section in the laser machine serves to shape the beam before allowing it to reach the mask. It comprises a number of optics to shape, collimate, homogenize and focus the beam.

A typical focusing arrangement is shown in Fig. 4. When a collimated beam passes through a double convex lens, it is converged on to a plane, called the *focal plane* of the lens. The point of convergence, also called the *focal point*, is in fact, not a point, but a spot. The spot, with the minimum radius of w_o, is called the *beam waist*. The minimum possible spot size, to which a beam can be practically focused, is called the *diffraction limited spot size*. Hence, while using mask projection, it is generally not possible to focus a beam to a size smaller than its diffraction limited spot size.

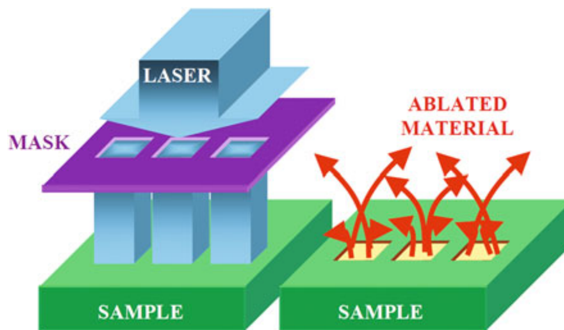

Fig. 3 Schematic of a mask projection setup, showing the incident laser beam, passing through a mask with *three square holes*, before falling on the work piece and ablating a similar pattern on it [Reprinted with permission, Rizvi (1999)]

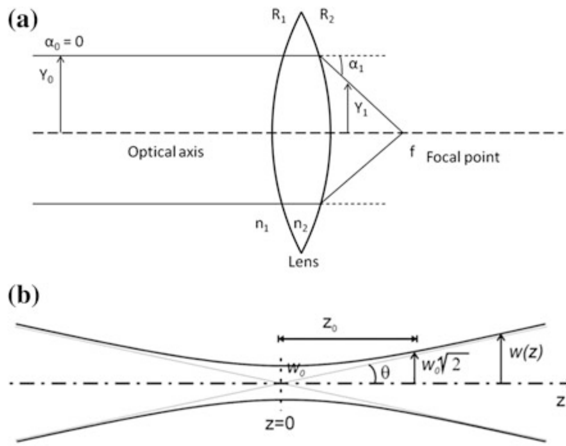

Fig. 4 Schematic diagrams of a simple optical system showing the convergence of a beam onto a focal plane, with a detailed description of the beam waist. **a** A focusing arrangement with a double convex lens. '*f*' is the focal point, lying on the optical axis '*z*'. **b** Enlarged view of the focal region, showing the beam waist with a radius of 'w_o', and Rayleigh range 'z_o'

Lasers with smaller wavelengths can be focused to smaller spots, and vice versa. Hence, it is advantageous to use lasers with small wavelengths (typically in the ultraviolet range) while fabricating micrometer sized features. The spot radius at the beam waist, w_o, is expressed as,

$$w_0 = \frac{4\lambda f}{2\pi y_0} \tag{3}$$

The Rayliegh range, z_o, is the distance along the optical axis, on either side of the beam waist, at which the beam diameter reaches 1.414 times its value at the beam waist. It is expressed as

$$z_0 = \frac{\pi w_0^2 M}{\lambda} \tag{4}$$

In the expressions above, λ is the wavelength of the laser, M is the beam quality factor, and f is the focal length of the lens. In a laser machining setup with mask projection, the workpiece is kept at the image plane of the mask, with the required placement accuracy of the order of the Rayleigh range. If the workpiece is not properly positioned, a blurred image of the mask features is obtained on the workpiece.

Mask projection employs a mask, which is generally a screen with transparent and opaque portions. The laser beam is allowed to pass through the transparent portion, and the shape of the transparent portion is machined/imprinted on the workpiece by virtue of its ablation. An example of a mask projection setup is shown in Fig. 5.

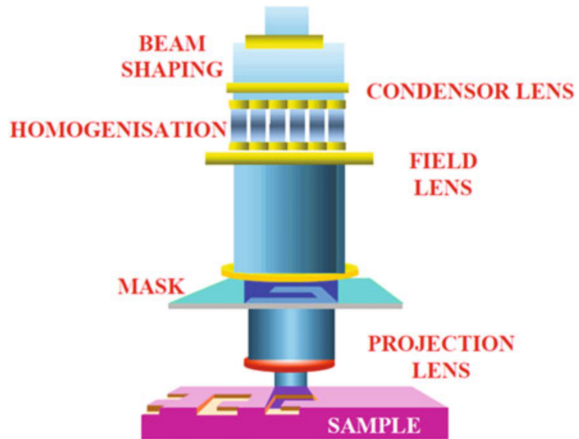

Fig. 5 Schematic of a mask projection system [Reprinted with permission, Rizvi (1999)]

The mask projection technique is a contrast to the direct write technique, and offers several advantages over the latter. The mask and the optics, being away from the work piece, do not suffer any damage due to ablation. Many setups allow movement of the mask as well as the work piece. The combination of mask and work piece scanning provides the ability to produce several complicated features, like arrays of micro features, nested holes, micro-channels with different kinds of cross sections etc. Since an image of the mask is used to machine micro features, it is possible to de-magnify the image and machine features that are much smaller than those on the mask. Demagnifications of 2X, 5X and 10X are widely used. The demagnification allows use of much lower fluences on the mask, thereby saving the mask from laser induced damage.

Several kinds of masks are used in the industry. Binary masks are the most widely used and easiest to fabricate. These generally contain either opaque elements deposited on a transparent substrate, or a pattern cut out on an opaque sheet of polymer or metal. These are similar to lithographic masks, but are more resistant to damage, primarily caused due to laser. Gray scale masks are another kind of masks that have varying transmissivity over the cross section. The smoothly varying transmissivity allows fabrication of smooth profiles on the workpiece. These are however much more difficult to fabricate and require calibration of transmissivity to produce desired patterns. Phase shift masks employ interference between portions of a beam passing through two separate regions of the mask, each with a different refractive index. Fine patterns with high contrast and resolution can be produced on the workpiece using such masks, but the masks require complex fabrication. Since binary masks are easy to fabricate, these are mostly used for producing micro features on polymer surface. In the following section we shall present a method to fabricate micro lens array with the help of a binary mask.

6 Fabrication of Micro Lens Array

In recent years the fabrication of micro lenses has gained attention of researchers. These micro lenses have found use in a plethora of components such as CCD arrays (Gale et al. 1997), digital projectors, 3D imaging (Hess 1912), and integral photography (Lippmann 1908). Moreover, current research indicates that array of micro lenses has the ability to act as concentrators for high efficiency photovoltaics (Karp et al. 2010). They are also used to couple light to optical fibres (Cohen et al. 1974). Therefore, the use of micro lenses in compact high performance micro optical devices has become essential. That is why, in the past decade, researchers have emphasized on deriving novel methods to fabricate lenses with lens diameter ranging from a few to several hundred micrometers.

Thus, there is a growing need to establish a cost effective, less complex and efficient method to fabricate micro-lenses. For the past two decades, researchers have been exploring various methods to fabricate refractive micro lenses. Some research was based on glass based lenses, while the study on polymer based lenses has opened a whole new window of opportunities. The photo-resist reflow method (Popovic et al. 1988), ultraviolet curing of polymer (Okamoto et al. 1999), LIGA method (Sankur et al. 1995), micro jet technique (MacFarlane et al. 1994) and micro moulding or hot embossing method (Ong et al. 2002) are some such new techniques which are used to fabricate micro lenses. However, these methods suffer from poor surface quality of features that cannot be improved. Hence, the use of these methods is restricted to some extent. Excimer laser micromachining has an important role in the fabrication of polymer based micro lenses as it interacts via photo-chemical mechanism or the cold ablation mechanism and therefore the surface quality can be controlled accurately (Brannon 1990; Dyer et al. 1985). The material is removed by laser ablation while the shape of the pattern is controlled by mask projection of laser source and the motion of a micro positioning stage.

For fabricating a 3-dimensional micro structure, one can use a photo mask which modulates the spatial laser intensity on the work piece, producing features of varying depth (Tien et al. 2003). Another method is known as contour mask scanning (Zimmer et al. 2000), in which contour or mask opening is synchronized with sample movement to achieve depth variation.

Lee et al. (2005) have successfully fabricated axis symmetric micro lenses using a new approach termed as “planetary mask contour scanning method”. In this method the mask revolves as well as rotates at the same time. The underlying principle is to create a probability distribution of laser intensity with the help of a self spinning mask which revolves around the sample producing axis symmetric feature. Authors have used 0.5 mm polycarbonate samples. According to the principle, the motion of the sample stage and mask revolution should be synchronized with laser firing sequence and before machining the mask centre should be in alignment with the sample stage. Lee et al. (2007) used this method to fabricate axis symmetric micro lenses of 200 μm aperture with high surface quality, i.e. surface roughness ranged from 3 to 6 nm.

Although several methods have been proposed over the years but still a systematic study and derivation of less complex and accurate method is required. In this paper we present a systematic study of fabrication process of micro lenses via use of a contour mask and work piece scanning.

6.1 Experimental Setup

A 248 nm KrF Excimer laser (Coherent Variolas Compex Pro 205F) is used for machining the micro lens array. The machine can deliver pulses of energy up to 750 mJ with 20 ns pulse width. The energy of the pulse can be varied by changing the discharge voltage or by manually tuning the attenuator. A pair of 8 × 8 fixed array of insect eye lenses is used to create a square field of 20 mm × 20 mm with homogeneous top hat beam profile at the mask plane. The setup for mask projection is shown in Fig. 6. The beam transmitted across the mask is imaged on the work piece through an imaging lens which has a demagnification of 10X. Optical microscopes and proprietary image analysis software have been used to capture and analyze the images. The work piece is an 8 mm thick piece of poly(methyl methacrylate) (also known as PMMA).

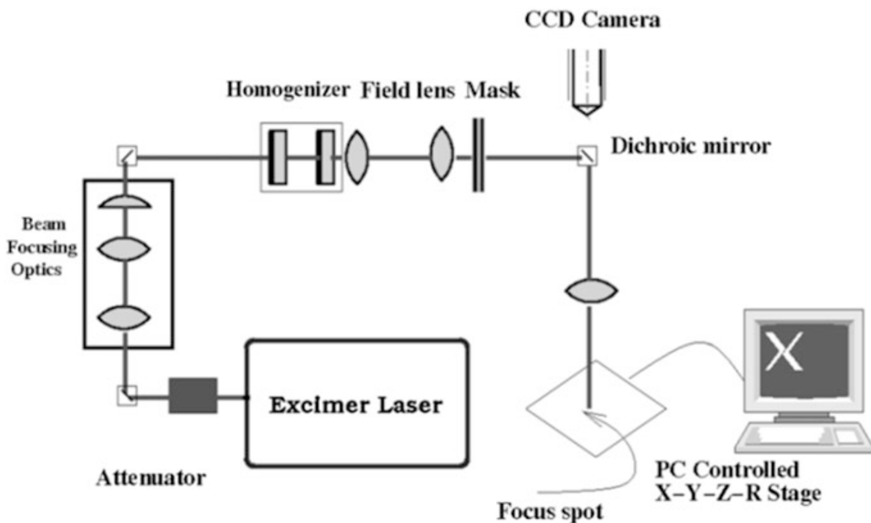

Fig. 6 Schematic of the experimental setup [from Dayal et al. (2013), reprinted with permission]

Table 4 Machining parameters and their values used in the experiments

Pulse energy (mJ)	176
Pulse repetition rate (Hz)	5
Scanning speed (μm/s)	8.3, 16.7, 25.0, 33.3

6.2 Experimental Procedure

The fabrication of micro lens array proceeds through generation of masks in two stages, followed by the fabrication of the lenses. The first stage mask used was a 30 mm × 30 mm piece of aluminium foil inside which the desired cross-sectional profile of the lenses was cut, at a scale of 100X. This mask was used to further machine the same profile, albeit at a 10 times smaller scale, on a polymer sheet. The polymer mask was finally used to fabricate the lenses on the PMMA work piece. The work piece was kept on a micro-positioning XYZ stage, and scanned along the X and Y axes to generate the lens array.

The machining parameters used for the experiments are mentioned in Table 4. The pulse energy was fixed at 176 mJ and the pulse repetition rate was fixed at 5 Hz. A set of experiments was conducted by varying the scanning speed of the work piece. The variation in scanning speed causes a variation in the number of pulses falling at a particular spot, and thereby varies the depth to which the feature gets machined.

7 Result and Discussion

7.1 Analysis of Masks

The first stage mask was fabricated in a piece of aluminium foil, and is shown in Fig. 7. The profile of the mask was designed in a way that the exposed length is largest at the center and it reduces, by second order, towards the periphery. This allows the manufacture of two halves of a lens, with peaks at the periphery and valley in the middle. Note that the region that has a larger exposed length sees more number of pulses per spot, and hence experiences greater machining depth.

The maximum exposed lengths in the first and second stage masks are 18.095 and 1.579 mm respectively, which is a reduction of about 11.5X. Clearly, an overcut of about 12.7 % is observed, which is expected in a laser machining process. The radius of the curved profile, has been reduced 10 times, as can be seen from Fig. 7.

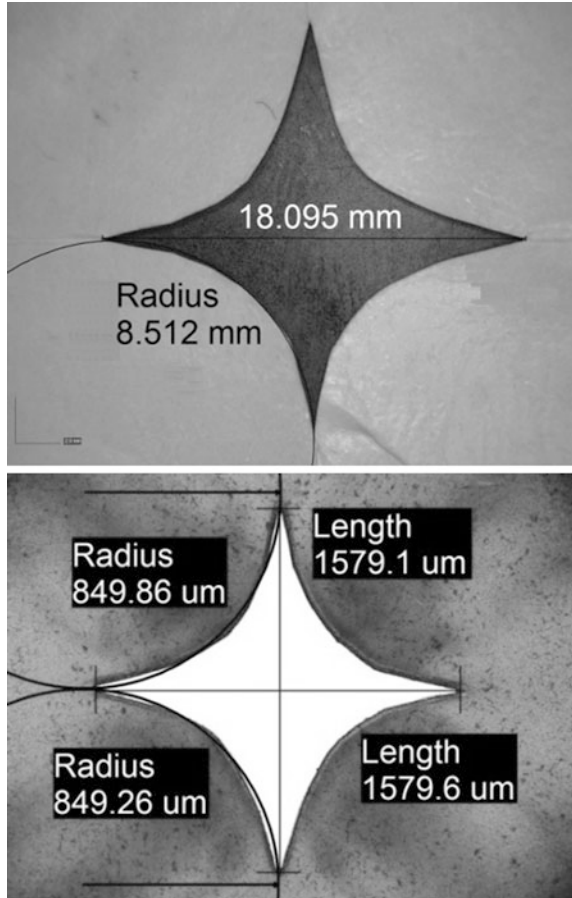

Fig. 7 First (*top*) and second (*bottom*) stage masks

7.2 Analysis of Micro Lens Profiles

The cross-sectional micrographs of the various lenses are shown in Fig. 8. Arrays of 3 × 3 lenses have been fabricated and their profiles are measured and compared with the theoretical profile expected from machining in PMMA. Note that it is easy to extend the size of the array to 10 × 10 or 100 × 100. The dimensions shown on the top of each figure (e.g. see Fig. 8a) show the depth to which the entire array has been machined. This depth is compensated for when comparing these profiles with the theoretical profile.

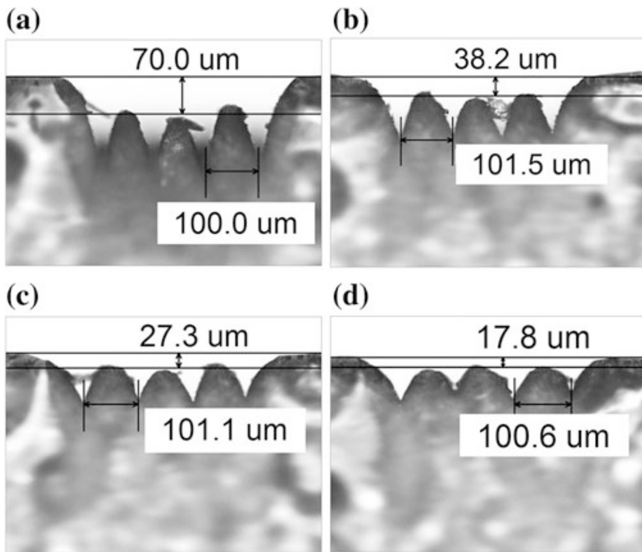

Fig. 8 Cross-sectional micrographs of lenses machined at various scanning speeds, **a** 8.3 µm/s, **b** 16.7 µm/s, **c** 25.0 µm/s and **d** 33.3 µm/s, with 176 mJ pulses and at 5 Hz. The adjacent lenses have been fabricated after indexing the work piece by 100 µm

7.2.1 Measurement of Ablation Rate of PMMA

Basic experiments were conducted on PMMA to measure the depth of ablation. Depths were measured after machining with several pulses of laser at three different pulse energies (120, 175 and 225 mJ). It is important that these measurements are done with several pulses so that incubation effects of photon absorption are compensated for, and the ablation depth per pulse reaches a steady value. Figure 9 shows the plot of ablation depth per pulse at the three different pulse energies, for varying number of pulses. As is widely reported, the etch depth per pulse varies

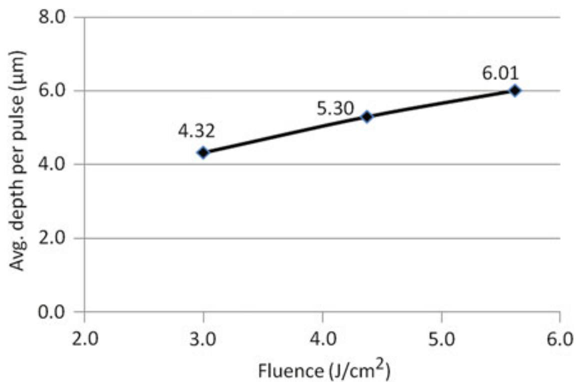

Fig. 9 Ablation rate of PMMA versus fluence

linearly with the fluence. A value of 5.3 μm/pulse is obtained for the pulse energy used (175 mJ). This value is used further to determine the theoretical profile of the lenses machined on PMMA.

7.2.2 Calculation of Theoretical Profile

In order to determine the theoretical profile of the lenses, it is important to determine the number of pulses that fall at each spot on the work piece. More number of pulses generates a greater depth. The number of pulses at a spot is determined by the scanning speed of the workpiece (s), the repetition rate of the laser (r) and the feature size (exposed length, l), in the direction in which the work piece is being scanned. In Fig. 10, the origin of coordinates is fixed at the point ‘O.’ The vertical distance to the bottom profile, from the horizontal axis, at a distance ‘X’ from ‘O,’ is calculated (P_0 P_1, as shown in the figure). The exposed length, L, is then, twice of this distance, and is expressed as

$$L = 2\left(R - \sqrt{R^2 - X^2}\right), \tag{5}$$

If the distance moved by the stage in 1 s is ‘s’, then ‘s’ units of length see ‘r’ pulses in a second. Hence, the number of pulses per spot will be the number of pulses falling per ‘L’ units of length, and is expressed as Eq. 6. The ideal depth of ablation is, then, given by,

$$pulses\,per\,spot = \frac{rL}{s}. \tag{6}$$

$$\text{Ideal depth} = \text{Pulses per spot} \times \text{ablation rate}. \tag{7}$$

The ideal depth of ablation helps to generate the theoretical profile of the lens. The theoretical profiles for all four cases of scanning speed are shown in Fig. 11.

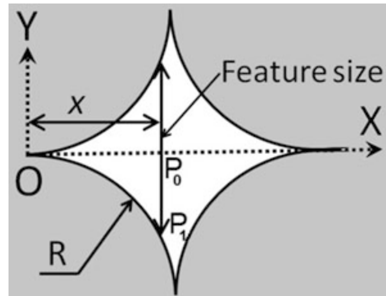

Fig. 10 Schematic of the procedure to calculate the feature size (exposed length)

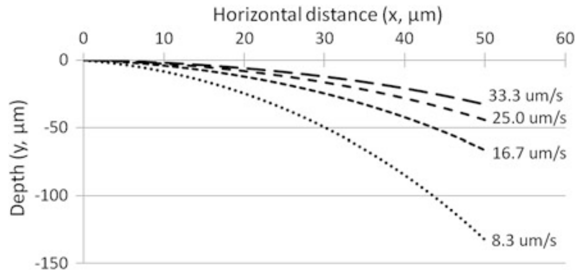

Fig. 11 Theoretical profiles of lenses machined at different scanning speeds

7.2.3 Micro Lens Profile—Experimental Results

Figure 12 shows the experimentally determined profiles of micro lenses in comparison with the theoretically predicted ones. All features show conformance to the theoretical profile to a very high degree. It can be noted that lenses machined at higher scanning speeds have lower machined depths. This is because lesser number of pulses fall per spot at a higher speed. Figure 13 shows the surface profiles of the machined lenses for the case of scanning speed of 33.3 μm/s.

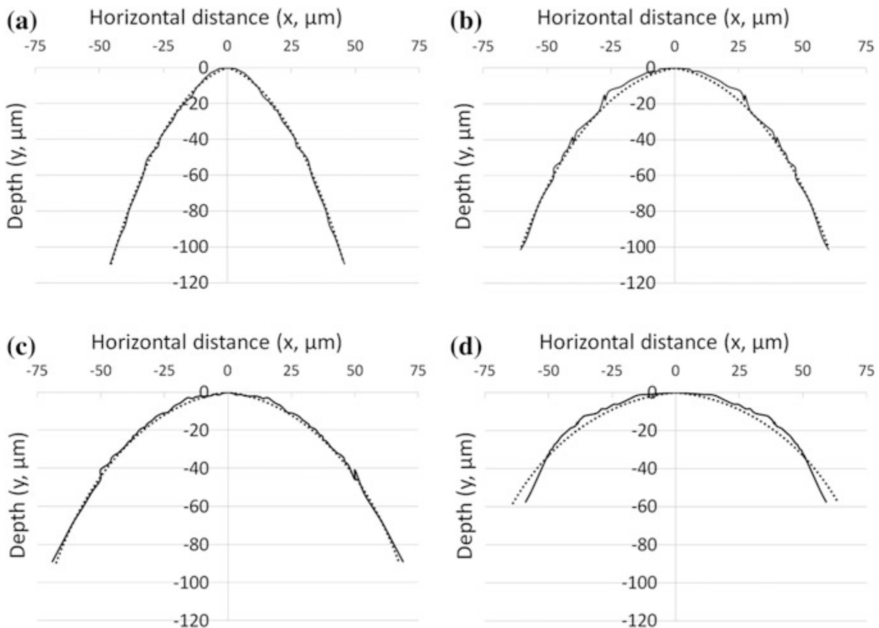

Fig. 12 Experimental and theoretical profiles of micro lenses plotted for varying scanning speeds, **a** 8.3 μm/s, **b** 16.7 μm/s, **c** 25.0 μm/s and **d** 33.3 μm/s (*Solid line*—experimental, *dotted line*—theoretical)

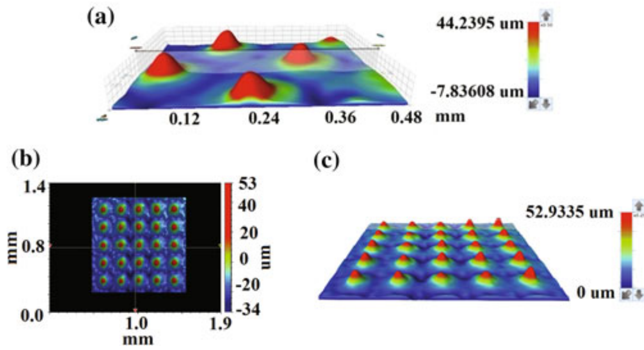

Fig. 13 3D Optical profilometery images of 5 × 5 array of micro lenses fabricated at the scanning speed of 33.3 µm/s. **a** Side view (closeup) of the micro lenses. **b** Micro lens array, fabricated over 1 mm × 1mm, when viewed from the top. **c** Side view of the micro lens array

8 Conclusions

Excimer laser micromachining has provided a new method to fabricate micro lens arrays. Therefore, it is important to study the various fabrication methods and their effects on feature quality. The effect of scanning speed and mask pattern is reviewed in this paper. At moderate scanning speeds the experimental profile agrees with the theoretical feature accurately. The number of pulses per spot is high at low scanning speeds. Hence, lenses are machined to a greater depth at low scanning speeds.

Acknowledgments The authors thank Dr. Nadeem Rizvi and ASME, SPIE and Elsevier for permissions to use some figures and tables in this chapter.

References

Akhtar, S. N., Ramakrishna, S. A., & Ramkumar, J. (2013). Excimer laser micromachining on polymers under different atmospheres and at different length scales. In *8th International Conference on Micro Manufacturing (ICOMM)*, March 25–28, Victoria, Canada.

Brannon, J. H. (1990). Excimer-laser ablation and etching. *IEEE Circuits and Devices Magazine, 6* (5), 18–24.

Choudhary, H. (2012). Numerical simulation and experiments of nano pulsed UV laser on metal and polymer (Master's thesis, Indian Institute of Technology Kanpur, Kanpur, India).

Cohen, L., & Schneider, M. (1974). Microlenses for coupling junction lasers to optical fibers. *Applied Optics, 13*(1), 89–94.

Dayal, G., Akhtar, S. N., Ramakrishna, S. A., & Ramkumar, J. (2013). Excimer laser micromachining using binary mask projection for large area patterning with single micrometer features. *ASME Journal of Micro and Nano Manufacturing*, *1*(3), 031002-1–7.

Dijkkamp, D., Gozdz, A., Venkatesan, T., & Wu, X. (1987). Evidence for the thermal nature of laser-induced polymer ablation. *Physical Review Letters, 58*, 2142–2145.

Dyer, P. (2003). Excimer laser polymer ablation: Twenty years on. *Applied Physics A, 77*, 167–173.

Dyer, P. E., & Sidhu, J. (1985). Excimer laser ablation and thermal coupling efficiency to polymer films. *Journal of Applied Physics, 57*(4), 1420–1422.

Feng, Y., Liu, Z., & Yi, X. (2000). Co-occurrence of photochemical and thermal effects during laser polymer ablation via a 248-nm excimer laser. *Applied Surface Science, 156*, 177–182.

Gale, M. T., Pedersen, J., Schütz, H., Povel, H., Gandorfer, A., Steiner, P., & Bernasconi, P. N. (1997). Active alignment of replicated microlens arrays on a charge coupled device imager. *Optical Engineering, 36*(5), 1510–1517.

Hess, W. (1912). Improved manufacture of stereoscopic pictures. UK Patent 13, 034.

Jensen, M. (2004). Laser micromachining of polymers (Ph.D. thesis, Technical University of Denmark, Denmark).

Karp, J. H., Tremblay, E. J., & Ford, J. E. (2010). Planar micro-optic solar concentrator. *Optics Express, 18* (2), 1122–1133.

Kűper, S., Brannon, J., & Brannon, K. (1993). Threshold behavior in polyimide photoablation: Single-shot rate measurements and surface-temperature modeling. *Applied Physics A, 56*, 43–50.

Lee, Y. C., & Wu, C. Y. (2007). Excimer laser micromachining of aspheric micro lenses with precise surface profile control and optimal focusing capability. *Optics and Lasers in Engineering, 45*, 116–125.

Lee, Y. C., Chen, C. M., & Wu, C. Y. (2005). A new excimer laser micromachining method for 3D microstructures with continuous surface profiles. *Sensors Actuators A, 117*(2), 349–355.

Lippmann, G. (1908). Epreuves reversibles. Photographies integrales. *Comptes Rendus, 146*, 446–451.

MacFarlane, D. L, Narayan, V., Tatum, J. A, Cox, W. R., Chen, T., & Hayes, D. J. (1994). Microjet fabrication of microlens array. *IEEE Photonics Technology Letters*, *6*(9), 1112–1114.

Meijer, J. (2004). Laser beam machining (LBM), state of the art and new opportunities. *Journal of Materials Processing Technology, 149*, 2–17.

Meijer, J., Du, K., Gillner, A., Hoffmann, D., Kovalenko, V., Masuzawa, T., et al. (2002). Laser machining by short and ultrashort pulses, state of the art and new opportunities in the age of the photons. *CIRP Annals-Manufacturing Technology, 51*, 531–550.

Okamoto, T., Mori, M., Karasawa, T., Hayakawa, S., Seo, I., & Sato, H. (1999). Ultraviolet-cured polymer microlens arrays. *Applied Optics, 138*, 2991–2996.

Ong, N. S., Koh, Y. H., & Fu, Y. Q. (2002). Microlens array produced using hot embossing process. *Microelectronic Engineering, 60*(3–4), 365–379.

Popovic, Z. D., Sprague, R. A., & Connell, G. A. (1988). Technique for monolithic fabrication of microlens arrays. *Applied Optics, 27*(7), 1281–1284.

Ready, J. (1965). Effects due to absorption of laser radiation. *Journal of Applied Physics, 36*, 462–468.

Rizvi, N. H. (1999). Production of novel 3D microstructures using excimer laser mask projection techniques. *Proceedings of SPIE, 3680*, 546–552.

Sankur, H. O., Motamedi, E., Hall, R., Gunning, W. J., & Khoshnevisan, M. (1995). Fabrication of refractive microlens arrays. *Proceedings of SPIE, 2383*, 179–183.

Srinivasan, R., Hall, R., Loehle, W., Wilson, W., & Allbee, D. (1995). Chemical transformations of the polyimide Kapton brought about by ultraviolet laser radiation. *Journal of Applied Physics, 78*, 4881–4887.

Srinivasan, R., Braren, B., Dreyfus, R., Hadel, L., & Seeger, D. (1986). Mechanism of the ultraviolet laser ablation of polymethyl methacrylate at 193 and 248 nm: laser–induced fluorescence analysis, chemical analysis, and doping studies. *Optical Society of America B, 3* (5), 785–791.

Tien, C. H., Chien, Y. E., Chiu, Y., & Shieh, H. D. (2003). Microlens array fabricated by excimer laser micromachining with gray-tone photolithography. *Japanese Journal of Applied Physics*, *42*(Part 1, No. 3), 1280–1283.

Tsutsumi, N., & Kiyotsukuri, T. (1988). Measurement of thermal diffusivity for polymer film by flash radiometry. *Applied Physics Letters, 52*, 442–444.

Zimmer, K., Braun, A., & Bigl, F. (2000). Combination of different processing methods for the fabrication of 3D polymer structures by excimer laser machining. *Applied Surface Science, 154–155*, 601–604.